Response of modern fluvial sediments to regional tectonic activity along the upper Min River, Eastern Tibet

Wei Shi[1, 2], Hanchao Jiang[1, 2, *], Hongyan Xu[1, 2], Siyuan Ma[1], Jiawei Fan[1, 2], Siqi Zhang[1], Qiaoqiao Guo[1], Xiaotong Wei[1]

[1]*State Key Laboratory of Earthquake Dynamics, Institute of Geology, China Earthquake Administration, Beijing 100029, China*

[2]*Lhasa Geophysical National Observation and Research Station, Institute of Geology, China Earthquake Administration, Beijing 100029, China*

Corresponding author: Hanchao Jiang, E-mail: hcjiang@ies.ac.cn

14   **Abstract**

15   The deposition of fluvial sediments in tectonically active areas is mainly controlled

16   by tectonics, climate, and associated Earth surface processes; consequently, fluvial

17   sediments can provide a valuable record of changes in regional climate and tectonic

18   activity. In this study, we conducted a detailed analysis of the grain-size distribution in

19   modern fluvial sediments from the upper Min River, Eastern Tibet. These data,

20   combined with information of regional climate, vegetation, hydrology, geomorphology,

21   lithology, and fault slip rate, indicate that modern regional tectonic activity along upper

22   Min River can be divided into three segments. Specifically, fluvial sediments in

23   Minjiangyuan - Diexi segment are dominated by silts (<63 μm, 70.2%), agreeing with

24   a low-runoff, low-rainfall and high vegetation cover and revealing a windblown origin

25   influenced by the arid and windy climate. These observations are consistent with the

26   low hillslope angle and low relief, all indicating weak activity along the Minjiang Fault.

27   The coarse-grained fraction (>250 μm) of fluvial sediments in Diexi - Wenchuan and

28   Wenchuan - Dujiangyan segments increases stepwise downstream, although runoff and

29   rainfall do not change significantly. These patterns correlate well with increases in both

30   regional relief and hillslope angles. Together, these observations imply that regional

31   tectonic activity along Maoxian-Wenchuan Fault becomes more pervasive downstream

32   along the Min River. The occurrence of well-sorted and well-rounded pebbles of fluvial

33   sediments in downstream of Dujiangyan must be related to the long-time scouring and

34   sorting by rivers. This study marks the first development of a new research approach

35   that can characterize regional tectonic activity by analysis of grain-size distribution of

36 fluvial sediments collected from tectonically active regions.

38 **Keywords:** Modern fluvial sediments; Grain-size analysis; Tectonic activity; Upper

39 Min River; Eastern Tibetan Plateau

1 Introduction

Tectonic geomorphology is a relatively young sub-discipline of geomorphology, and has the major aim of unraveling interactions between tectonic activity, climate, and Earth surface processes (Wobus et al., 2005; Owen, 2013). The grain-size distribution of river bed material, channel width, channel sinuosity, extent of alluvial cover, lithology of bedrock, and hydraulic roughness are all potentially important variables (Whipple, 2004; Whittaker et al., 2010). Although many factors determine the grain-size distribution of fluvial sediments, but there are one or two mainly controlling factors in specific regions. Previous studies have shown that it is feasible to discuss the main control factors for changes in grain-size of fluvial sediments (Singh et al., 2007; Bravard et al., 2014). In addition, comprehensive amounts of data must be collected in a wide range of field settings before the responses of these important variables to climatic and tectonic forcings can be determined.

The topographic margin of the Tibetan Plateau (TP) along the Longmen Shan is one of the most impressive continental escarpments in the world, and the land surface rises westward over a horizontal distance of 40–60 km from the Sichuan Basin (500–700 m elevation) to peak elevations exceeding 6000 m (Chen et al., 2000; Kirby et al., 2000, 2008). Some studies have revealed common topographic features within river channels in the eastern TP, namely, an upper low-gradient channel segment, a middle steep-gradient channel segment, and a lower very steep channel segment, such as in the Red River region in Yunnan Province (Schoenbohm et al., 2004) and the Min River region in Sichuan Province (Kirby et al., 2003). However, it is important to note that strong lithological contrasts along the river can also cause the channel steepness index

to change at comparable magnitudes to those associated with large gradients in rock uplift rate (Snyder et al. 2000; Beek and Bishop, 2003; Stock and Dietrich, 2003; Whittaker et al., 2010). New data sourced from several localities record an apparent narrowing of channel width in response to increased rock uplift rates in rivers with large areas of bedrock (Whipple, 2004). This is consistent with the recent proposition that river profiles straighten as aridity increases (Chen et al., 2019), as observed along the upper Min River in the field. Generally, exposures of hard bedrock often generate straight channels, which have low channel slopes and small sediment loads (Schumm and Khan, 1971, 1972).

Vegetation density can modulate topographic responses to changing denudation rates, such that the functional relationship between denudation rate and topographic steepness becomes increasingly linear as vegetation density increases (Olen et al., 2016). Recent studies indicate that the upper Min River has poor vegetation coverage and most regions are fully exposed due to the strongly arid climate conditions (Jiang et al., 2015; Shi et al., 2020; Xu et al., 2020; Wei et al., 2021; Zhou et al., 2021). Thus, hillslope colluvium is the dominant sediment source to the upper Min River - especially in its middle and lower parts (Zhang et al., 2021) - akin to those in drainage basins in many arid regions worldwide (Clapp et al., 2002).

Tectonic activity influences the evolution of lacustrine sedimentary sequences by affecting the provenance supply (Najman, 2006; Jiang et al., 2022). Frequent earthquakes on the TP, as recorded by widely distributed soft sediment deformation (Wang et al., 2011; Xu et al., 2015; Jiang et al., 2016; Zhong et al., 2019; Zhang et al., 2021), caused repeated landslides that also represent another major source of sediment into the upper Min River (Dai et al., 2011; Xu et al., 2012, 2013). These landslides

generated a large amount of dust storms that deposited in nearby lakes (Jiang et al., 2014, 2017) and exposed large quantities of fine-grained sediment that had accumulated on mountain slopes, which were subsequently transported by wind to ancient lakes, documenting these seismic events (Whittaker et al., 2010; Liang and Jiang, 2017; Shi et al., 2022). This sedimentological process was recently recognized at Huojizhai, Diexi Town, following the 1933 M_s 7.5 Diexi earthquake (Wei et al., 2021).

Changes in hydrology and sediment flux are commonly regarded as climate forcing (Wobus et al., 2010). The alluvial cover is very limited throughout the upper Min River Basin, which is demonstrated by similarity of zircon U-Pb ages in lacustrine sediments and their nearby bedrock units (Zhong et al., 2017). As such, the influence of occasional flood events should be considered over a longer time scales (Snyder and Whipple, 2003), as aridity precludes rainfall or fluvial undercutting as triggers for such events.

The consistent climate coupled with systematic variations in lithology and rock uplift rate along the Min Mountains allow comparison of channels that experience different tectonic forcings (Duvall et al., 2004). Selective transport is the dominant downstream fining mechanism in this region, although rates of selective transport in sand-bed rivers are smaller than those in gravel-bed rivers (Frings, 2008).

Only a small volume of sediment collected from a river bed is needed to produce a transformative understanding of the rates at which landscapes change (Blanckenburg, 2005). Study of these materials can reveal relationships between generation, transport (Clapp et al., 2000, 2002), and mixing of sediment (Perg et al., 2003; Nichols et al., 2005), under the help of the key topographic and/or lithologic features (e.g., relief, slope angle, and substrate characteristics) (Riebe et al., 2000; Riebe et al., 2001; Matmon et al., 2003a, b). The Min River is one of the important tributaries of the Yangtze River

and goes through the climate transition zone and the tectonically active zone in the eastern TP. The alpine valleys along the Min River reduce the preservation potential of Quaternary sediments and expose large areas of bedrock, which hinder the study of tectonic activity. In this study, we combine field surveys and analysis of river sediments in the upper Min River to determine hydraulic characteristics, and topographic and tectonic information about bedrock channels.

2 Regional setting

2.1 Geographic and geologic settings

Instrumental data collected after 1900 indicate that the TP has experienced strong earthquakes clustered around the Bayan Kala Block from 1995 to the present, which are collectively known as the Kunlun-Wenchuan earthquake series (Deng et al., 2014). The eastern TP is tectonically controlled by the Longmen Shan thrust belts, the Minjiang Fault, and the Huya Fault (Fig. 1a). Frequent tectonic activities have led to numerous earthquakes and landslides in this region (e.g., Zhang et al., 2003; Jiang et al., 2014; Li et al., 2015; Liang and Jiang, 2017), such as the 1933 Diexi M_s 7.5 earthquake, the 1976 Songpan M_s 7.2 earthquake, the 2008 Wenchuan M_s 8.0 earthquake and the 2017 Jiuzhaigou M_s 7.0 earthquake, which caused widespread geomorphic landscape damage, and released a large amount of fresh terrigenous debris. The sudden coarsening of grain-size in the Xinmocun and Lixian lacustrine sections is considered to be related to earthquakes (Jiang et al., 2014, 2017). GPS-measured uplift rates in the Longmen Shan Fault zone reached 2–3 mm/a over 10 years since 1999 (Liang et al., 2013). Thermochronological dating of zircon and apatite indicated

136 denudation rates of 1–2 mm/a in the Longmen Shan region during the Late Cenozoic

137 (Kirby et al., 2002).

138
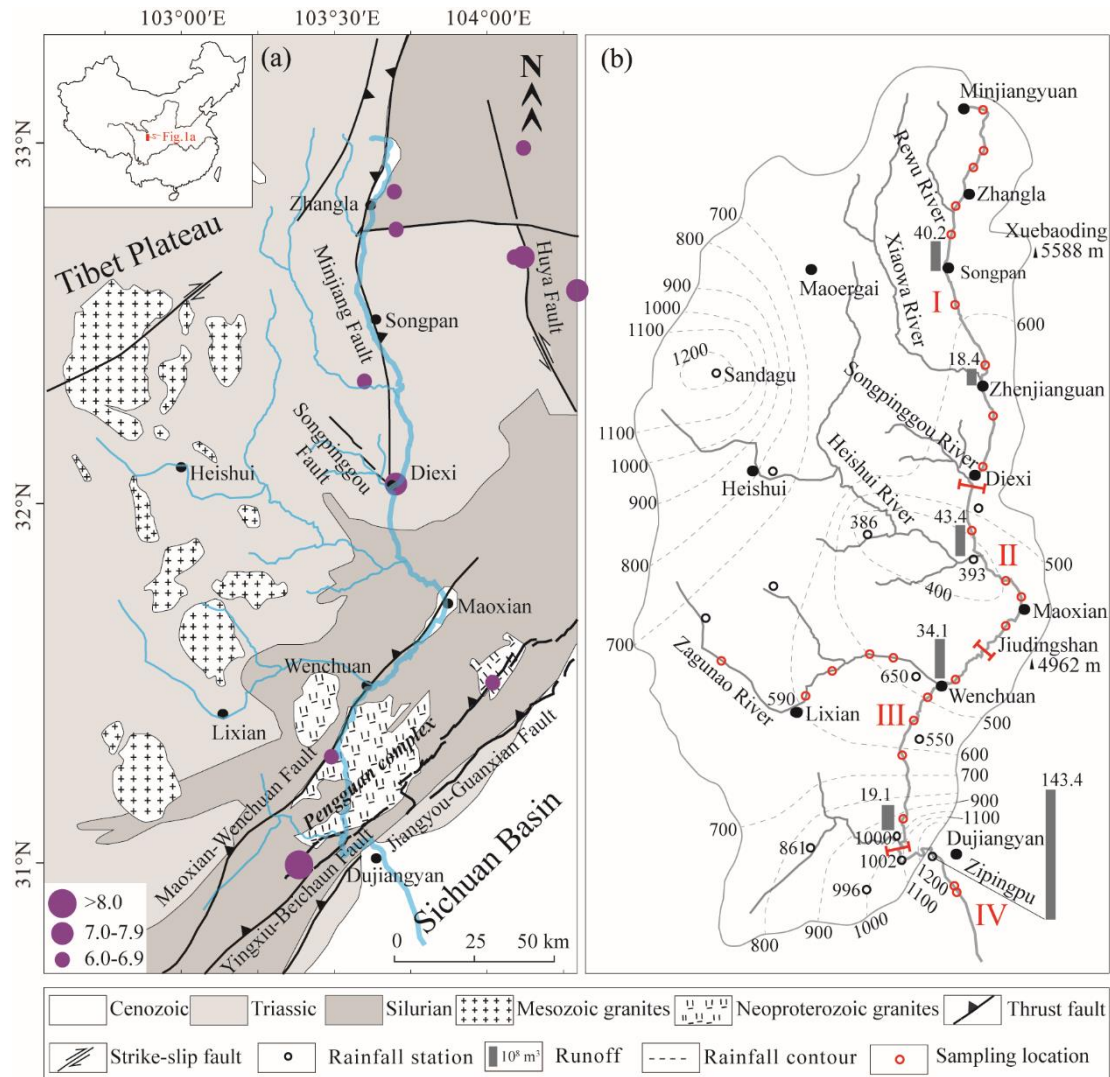
139 **Figure 1 (a)** Geological map and **(b)** precipitation distribution (Ding et al., 2014) for

140 the upper Min River basin. Seismic data are from the China Earthquake Data Center

141 (http://data.earthquake.cn/data).

142   Bedrock outcrops within the catchment region of the upper Min River are

143 dominated by Silurian phyllite, quartz schist, and Triassic phyllite, metamorphosed

144 sandstone (Fig. 1a), which are easily weathered and eroded into transportable debris

145 (Zhong et al., 2019). Massive granites are also exposed in the study area; in particular,

146 the Neoproterozoic Pengguan complex (U-Pb ages of 859–699 Ma; Ma et al., 1996)

147 (Fig. 1a) is mainly composed of intermediate-acid intrusive rocks, with lesser amounts

148 of basic-ultrabasic intrusive rocks, volcanic rocks, volcanoclastic rocks, and greenschist

149 facies metamorphic rocks. Sand (> 63 μm) in the study area was recently demonstrated

150 to have been mainly derived from local debris material, which itself is likely related to

151 dust storms and loose surface material produced by seismic activity (Jiang et al., 2017;

152 Liang and Jiang, 2017).

153   The upstream channel of the Min River is ~340 km long (Li et al., 2005; Ding et

154 al., 2014), nearly oriented N-S (Fig. 1b), and erodes the hinterland of the TP via

155 formation of gullies and valleys. The Min River valley is typically steep, narrow and

156 deepening downstream with an incision depth of 300–1500 m (e.g., Li et al., 2005;

157 Zhang et al., 2005). The slopes on both sides of the study area ranges from 18° to 45°,

158 and the vertical aspect ratio of the valley ranges from 5.5 to 12.6 ‰ (Zhang et al., 2005).

159 Constrained by the specific landforms of the alpine valleys, the wind direction in the

160 study area is generally SSW/NNE, roughly consistent with the strike of local valleys

161 (Liu, 2014). The Min River valley exhibits high wind speeds in April (mean 4.9 m/s)

162 and low speeds in July (mean 3.7 m/s). Wind speed is generally < 4 m/s before noon

163 and > 4 m/s after noon, and normally peaks approximately 8–10 m/s at around 16:00

164 (Liu, 2014). The highest instantaneous wind speed recorded in the study area was 21

165 m/s (Liu, 2014).

166   The upper reaches of the Min River are located in a transition zone on the TP

167 where wet monsoonal climate changes to a high-elevation cold climate. In this region,

168 mean annual precipitation (MAP) ranges from 400 mm to 850 mm, and precipitation is

169 dominant (>75%) during the rainy season (May-October) (Ding et al., 2014). It is

170 noticeable that orographic rain along the eastern TP generates two storm areas centered

171 around Sandagu and Zipingpu (Fig. 1b). Statistical analyses of precipitation data from

172 1982 to 2007 show that the MAP within these regions is higher than 1200 mm (Ding et

173 al., 2014).

174   Regional vegetation has clear vertical zonation, which mainly consists of small-

175 leaf, arid shrubs at 1300–2200 m a.s.l., mixed broadleaf-conifer forests, evergreen and

176 deciduous broad-leaved mixed forests at 2000–2800 m a.s.l., *Picea* and *Abies* forests at

177 2800–3600 m a.s.l., and alpine shrubs and meadows at > 3600 m a.s.l. (Ma et al., 2004).

178 There are two key factors that influence vegetation distribution and ecological

179 conditions in the study area: the arid and windy climate, which has a large temperature

180 difference between day and night, and tectonics activity characterized by frequent

181 earthquakes (Lin, 2008; Wang et al., 2011). For example, strong earthquakes often

182 induce landslides that can destroy vegetation cover in the study area (Xu et al., 2012,

183 2014). Both of these factors lead to fragility in landscape and vegetation cover.

184 **2.2 Segmented characteristics of the Min River**

185   Based on the topographical and geomorphological characteristics, fault and

186 vegetation distribution patterns, the upper Min River could be subdivided into four

187 segments (Fig. 1b).

188   Segment I is the Minjiangyuan - Diexi segment (3460–2190 m a.s.l.). The riverbed

189 in this segment is directly connected with one side of the Min Mountain and has a valley

190 bottom width of 200–1000 m (Zhang et al., 2005) (Fig. 2a). Downstream from

191 Minjiangyuan, valley bottom width narrows markedly and is only 200–300 m in

192 Zhenjiangguan - Diexi segment (Zhang et al., 2005). The relative relief of the Min

193 Mountain increases significantly from Minjiangyuan to Diexi along the Min River,

194 especially from Zhenjiangguan to Diexi (Zhang et al., 2005). The vegetation coverage

195 along this segment gradually deteriorates, with *Picea*, *Abies*, shrubs, and herbs in the

196 Minjiangyuan - Songpan segment, but only a small number of shrubs and herbs in the

Songpan - Diexi segment. Bedrock is widely exposed in the lower part of the segment.

In this region, the monthly maximum wind speed reaches 15.4 m/s in Songpan.
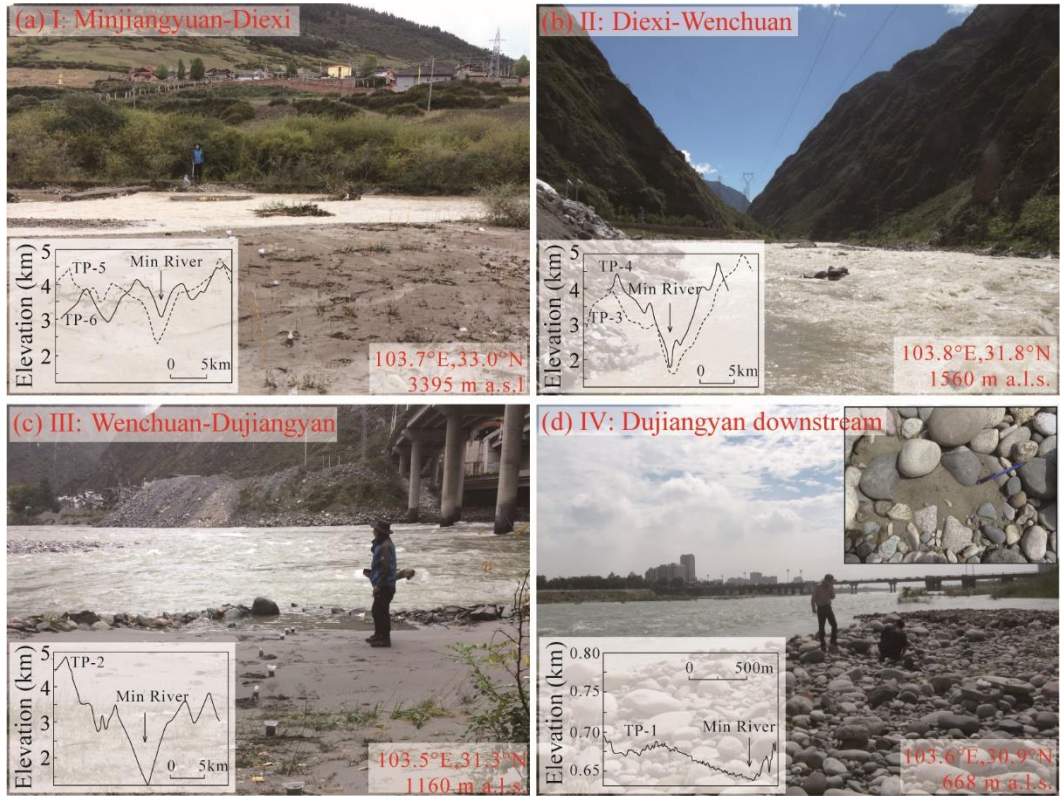
Figure 2 Photographs of field sampling sites in the upper Min River. The locations of cross-sections through the Min River valleys (Zhang et al., 2005) are shown in Fig. 7c.

Segment II is the Diexi - Wenchuan segment (2190–1470 m a.s.l.). The valley bottom width in this segment decreases to 200–300 m (Zhang et al., 2005), and the Min Mountains always occur in direct contact with the riverbed of the Min River (Fig. 2b). The longitudinal slope (12.6‰) reaches its maximum near Diexi (Zhang et al., 2005). The regional vegetation coverage is mostly sparse and the bedrock is well exposed.

Segment III is the Wenchuan - Dujiangyan segment (1470–900m a.s.l.). The valley bottom width in this segment widens to about 200–500 m (Zhang et al., 2005) (Fig. 2c) and regional vegetation cover increases compared to segment II. In particular, the hillside around the Zipingpu Reservoir is covered with thick broad-leaved trees and herbs. The monthly maximum wind speed in Lixian is 14.0 m/s.

212   Segment IV is the Dujiangyan downstream segment (900 – 630 m a.s.l.). This

213 segment flows into the interior of the Sichuan Basin, where it has flat geomorphological

214 features (i.e., the riverbed width is greater than 300 m; Fig. 2d), and then transitions

215 into the middle reach of the Min River. The monthly maximum wind speed in

216 Dujiangyan is 13.8 m/s.

217

218 **3 Materials and methods**

219 **3.1 Field sampling and grain-size analysis**

220   A ~340 km transect along the upper Min River was conducted during October

221 2017, starting in the eastern TP (Minjiangyuan, 33°01′59″N, 103°42′42″E; 3462 m a.s.l.)

222 and ending in the Sichuan Basin (Dujiangyan, 30°56′25″N, 103°38′14″E; 634 m a.s.l.)

223 (Fig. 1b). A total of 181 river samples were collected for grain-size analysis at 25 sites

224 (Table S1). Sampling sites were selected from exposed, freshly-developed depositional

225 sequences that occurred close to the active channel and its margins (Fig. 2). Voluminous

226 bedrock gravel occurs around the sampling sites (Fig. 2). To ensure sample consistency

227 associated with uniform flow regimes, each sample was collected at a depth of 0–0.2 m

228 from different locations in each sampling sequence. All locations were carefully chosen

229 to avoid contamination from riverbank materials or from anthropogenic reworking.

230   Grain-size analysis was conducted using a Malvern Mastersizer 3000 laser grain-

231 size analyzer at the State Key Laboratory of Earthquake Dynamics, Institute of Geology,

232 China Earthquake Administration in Beijing, China. About 0.5 g of sediment was

233 pretreated with 20 ml of 30% H_2O_2 to remove organic matter and then with 10 ml of

234 10% HCl to remove carbonates. About 300 ml of deionized water was added, and the

sample solution was kept for 24 h to rinse acidic ions. The sample residue was dispersed

with 10 ml of 0.05 M $(NaPO_3)_6$ on an ultrasonic vibrator for 10 min before grain-size

measurements. For each sample, the grain-size analyzer automatically outputs the

median diameter (Md) and the percentages of each size fraction, with a relative error of

less than 1%. Magnetic susceptibility (SUS) was measured using a Bartington MS2

susceptibility meter.

3.2 Y values

Mean grain size (Ms), standard deviation (σ), skewness (Sk), and kurtosis (K_G) are

commonly used to discriminate different depositional processes and environments.

Sahu (1964) distinguished aeolian processes from those that operate in a littoral

environment by using the following equation:

$$Y = -3.5688\,Ms + 3.7016\,\sigma^2 - 2.0766\,Sk + 3.1135\,K_G \tag{1}$$

Here, Y values less than -2.74 indicate an aeolian provenance and Y values greater

than -2.74 indicate a hydrogenic provenance (Sahu, 1964). Calculated Y values for

lacustrine sediments (Jiang et al., 2014, 2017), red clay, and loess-paleosol deposits (Lu

and An, 1999; Wu et al., 2017) are less than -2.74, indicating an aeolian provenance.

3.3 End-member analysis

Numerical unmixing of grain-size distribution data into constituent components,

known as end-member analysis (EMA), can yield valuable information about transport

dynamics (Weltje, 1997; Paterson and Heslop, 2015; Jiang et al., 2017). According to

the principle that the end-member number (EM) should be as small as possible (Weltje

et al., 1997), several EMs obtained by end-element analysis imply that numerous

dynamic mechanisms occurred during formation of these deposits. Generally, larger

values of EMs correspond to a stronger transport capacity, which indicates different

provenances (Vandenberghe, 2013; Dietze et al., 2014; Jiang et al., 2017). For instance,

the peak values of EMs in Lixian lacustrine sediments were concentrated at 10 μm (EM_1)

and 40 μm (EM_2), reflecting the background deposition of dust and locally sourced

deposition transported by ambient wind, respectively (Jiang et al., 2017). We analyzed

the Min River samples using the AnalySize software for processing and unmixing

grain-size data (Paterson et al., 2015), with the generalized Gaussian skewness model

(SGG) (Egli, 2003).

3.4 C-M and F-M diagrams

The analysis of C-M and F-M diagrams is useful to interpret sediment transport

dynamics (Passega, 1957; Singh et al., 2007). In these diagrams, C is the coarsest

percentile of the grain-size distribution in samples (one percentile), and M is the median

diameter of the grain-size distribution, which are both indicators of the maximum and

average transport capacity, respectively (Passega, 1957; Singh et al., 2007; Bravard et

al., 2014). In addition, F represents the percentage of fractions finer than 125 μm (Singh

et al., 2007). All values are plotted on a logarithmic scale, which produces specific

patterns for distinct reaches (Singh et al., 2007; Bravard et al., 2014). A C-M diagram

(Fig. S1) has the following sections: NO, rolling; OP, rolling with some grains

transported in suspension; PQ, graded suspension with some grains transported by

rolling; QR, graded suspension; RS, uniform suspension; and T, pelagic suspension

(Passega, 1957; Bravard and Peiry, 1999; Bravard et al., 2014).

4 Results

4.1 Characteristics of grain-size and SUS

The median grain size (Md), grain-size fractions (0-2 μm, 2-20 μm, 20-63 μm, 63-250 μm, >250 μm), SUS and Y values of the fluvial sediments can be divided into four segments (Fig. 3), which correspond to the different segments of the upper Min River (I - IV) defined above. The average values of Md increased significantly at Diexi (from 31.0 μm to 80.8 μm) and Wenchuan (from 49.3 μm to 170.2 μm), and decreased slightly at Dujiangyan (from 220.4 μm to 119.2 μm). The variations at these three sites are the most significant within the whole river (Table 1, Fig. 3).

Table 1 Statistics for grain-size fractions in the upper Min River.

Segments	Md (μm)	Percentage composition / (%)					SUS
		0–2 μm	2–20 μm	20–63 μm	63–250 μm	>250 μm	
I	31.0	2.8	40.3	27.1	23.7	6.2	11.6
II	80.8	0.4	25.3	20.3	34.6	19.4	11.3
III	170.2	0.3	20.0	13.9	31.9	33.8	193.5
IV	145.2	0.5	13.0	9.5	59.5	17.5	251.8
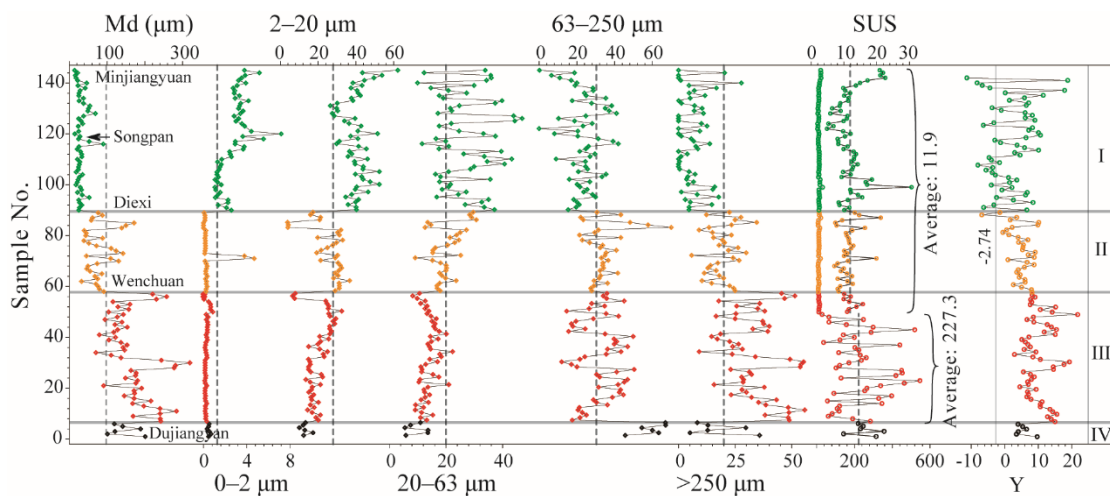
Figure 3 Variation of grain-size components and river sediment parameters from the upper Min River. The dotted lines represent the average value of the whole sequence.

294   Along the upper Min River downwards, the mean proportion of the 2–20 μm (I =

295   40.3%, II = 25.3%, III = 20.0%, and IV = 13.0%) and 20–63 μm fractions (I = 27.1%,

296   II = 20.3%, III = 13.9%, and IV = 9.5%) exhibit a stepwise decrease (Table 1, Fig. 3).

297   The 63–250 μm fraction exhibits a sharp increase from segment I (23.7%) to II (34.6%)

298   and from segment III (31.9%) to IV (59.5%), but a relatively minor change from

299   segment II (34.6%) to III (31.9%) (Table 1, Fig. 3). The > 250 μm fractions exhibit a

300   stepwise increase from segment I to III (6.2%, 19.4%, and 33.8%, respectively), and a

301   significant decrease from segment III (33.8%) to IV (17.5%) (Table 1, Fig. 3). SUS

302   values remained low in segments I (5.3–30.6, mean 11.6) and II (7.1 to 21.2, mean 11.3),

303   but were significantly higher in segment III (9.9–546.5, mean 193.5) and reached

304   consistently high values in segment IV (142.1–356.5, mean 251.8) (Table 1, Fig. 3).

305   **4.2 End-member analysis**

306   Three end-members (EMs) (R^2 = 0.93) were identified in the Min River samples

307   (Fig. 4) with peaks of 21.2 μm (58.0%), 185.8 μm (24.2%), and 351.7 μm (17.8%),

308   respectively. Along the upper Min River downwards, these three EMs show clear

309   stepwise changes between segments (Fig. 5). EM_1 shows a stepwise decrease (I = 82.5%,

310   II = 53.1%, III = 38.6%, and IV = 23.7%), corresponding to the sum of the 2–20 μm

311   and 20–63 μm fractions (Figs. 3, 5). EM_2 shows a sharp increase from segment I (13.1%)

312   to II (31.4%) and from segment III (27.1%) to IV (67.4%), and a relatively smaller

313   change from segment II (31.4%) to III (27.1%), corresponding to the 63–250 μm

314   fraction. By contrast, EM_3 corresponds to the >250 μm fraction (Figs. 3, 5) and shows

315   a stepwise increase from segment I to III (4.4%, 15.5% and 38.6%, respectively), and a

316   significant decrease from segment III (38.6) to IV (23.7%).
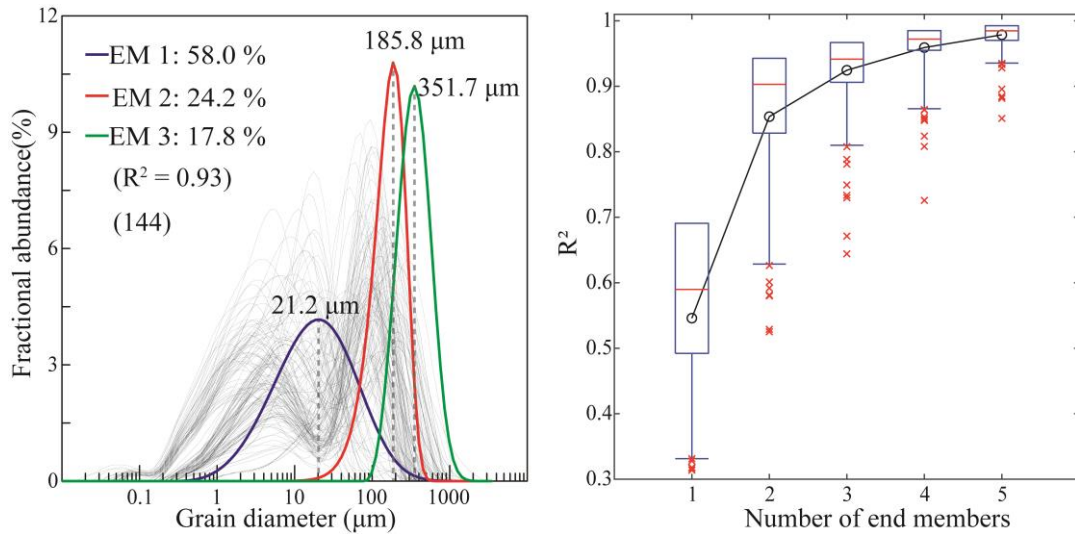
317   **Figure 4** End-member analysis model of fluvial sediments from the upper Min River.

318
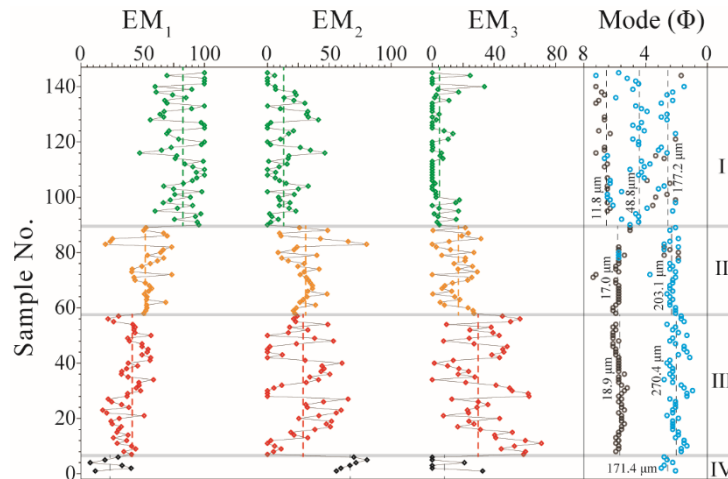
319   **Figure 5** Variability of EMs and mode values of fluvial sediments from the upper Min

320   River. The peak values (mode values) with >1% fractional abundance of the grain-size

321   frequency distributions were extracted after consideration of a 1% instrumental error.

322   Blue and gray circles represent the main and secondary peak modal values, respectively.

323   The dotted lines represent the average value.

324

325   **4.3 Characteristics of the grain-size frequency distribution**

326   The grain-size frequency of river samples from segment I has a discrete

327   distribution (Fig. S2) with three mode values at ~11.8 μm, ~48.8 μm, and ~177.2 μm.

328 The main mode value of segment I occurred in the ~48.8 μm portion. The grain–size

329 frequency distribution for segments II and III is strongly bimodal (Fig. S2), with the

330 major and minor mode values at ~203.1 μm and ~17.0 μm for segment II, and ~270.4

331 μm and ~18.9 μm for segment III. The grain-size frequency distribution for segment IV

332 is unimodal (Fig. S2) with a mode value of ~171.4 μm.
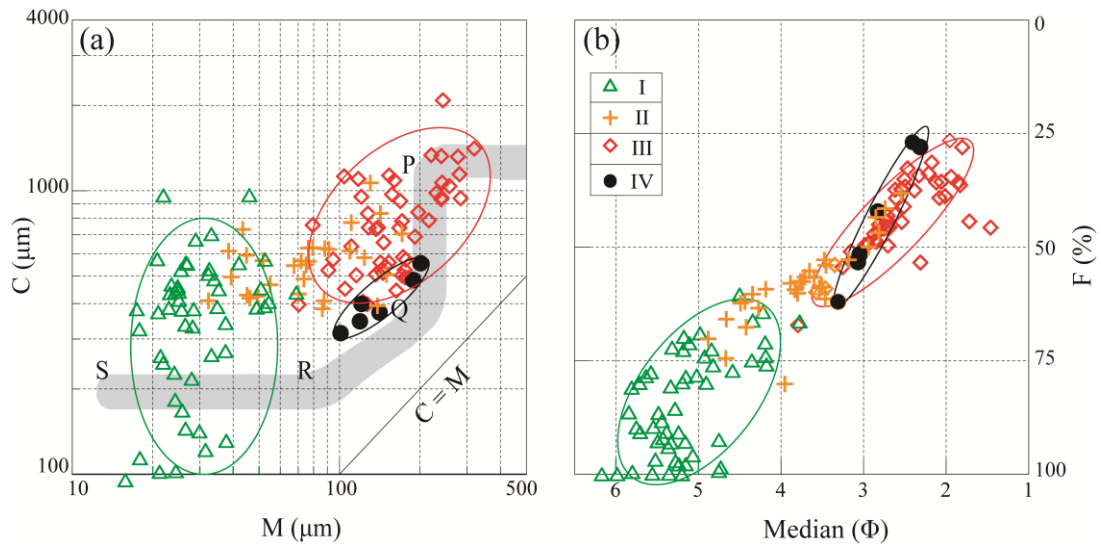
333 **Figure 6** C-M and F-M diagrams of fluvial sediments from the upper Min River.

334 **4.4 C-M and F-M diagrams**

335 On the C-M diagram, samples from segment I are completely separate from those

336 of segments III and IV. Most samples in segment II overlap with those of segment III

337 (Fig. 6a). Among them, the M value of segment I (13.9–89.8 μm) mainly belongs to the

338 RS section (Fig. 6a), although the C values exhibit a large variation between 54.8 μm

339 and 964.3 μm. Samples from segment II are distributed throughout the P-Q-R sections

340 (Fig. 6a), with C values of 383.5–1066.0 μm, and M values of 32.2–171.4 μm. Samples

341 from segment III are concentrated in the PQ section (Fig. 6a), with C values of 396.9–

342 2083.8 μm, and M values of 70.3–319.1 μm. Samples in segment IV plot close to the

RQ section and are distributed parallel to the C = M line (Fig. 6a). Fluvial sediments of the Min River show similar distribution features in F-M diagram to those in C-M diagram (Fig. 6).

5 Discussion

5.1 Dynamic and provenance implications of fluvial sediments

Grain-size fractions, EMs, and mode values in different segments along the upper reaches of Min River reflect the distinct provenance and transport dynamics of fluvial sediments (McKinney and Sanders, 1978; Sun et al., 2002, 2004; Sun et al., 2007; Vandenberghe, 2013; Dietze et al., 2014). The EM_1 in segment I reaches a proportion of 82.5%, which corresponds to the fine particle components (<63 μm fractions). Previous studies have indicated that fractions with sizes of <10 μm and 10–40 μm represent background particles and regional dust that have been transported by wind (Dietze et al., 2014; Jiang et al., 2014, 2017), which contribute 51±11% and 42±14% of the lacustrine sediments across the TP, respectively (Dietze et al., 2014). Therefore, the EM_1 (fine-grained fractions) in segment I probably have an aeolian provenance. This inference is supported by five separate lines of evidence: 1) Md varies in a narrow range of 13.9 to 89.8 μm (Fig. 3), although the C values fluctuate widely between 54.8 μm and 964.3 μm (Fig. 7); 2) the distribution of samples in RS section of the C-M diagram (Fig. 6) reflects uniform suspension, which likely requires transportation by ubiquitous and strong wind (Fig. S1, Passega, 1957); 3) nearly half of the samples (i.e., 22 out of 55) have Y values of less than –2.74, which is indicative of an aeolian origin

365 (Sahu, 1964); 4) loess deposits are widely distributed in the study area, especially from

366 Diexi upstream (Fig. S3) (Liu et al., 2013; Shen et al., 2017), which represent a

367 voluminous source of dust particles; and 5) the study area has a high mean altitude of

368 2840 m, and the monthly maximum wind speed can reach 15.4 m/s, which is conductive

369 to strong aeolian transport.
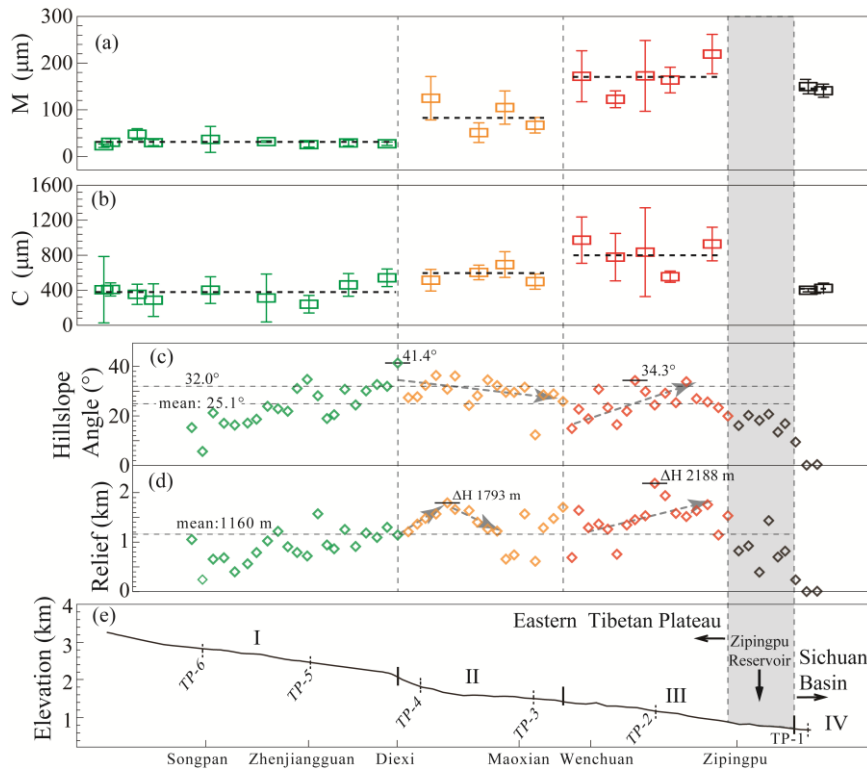
370 **Figure 7** Variation characteristics of **(a)** M and **(b)** C values of the grain-size index. **(c)**

371 Riverbed base-level and the position of the cross-section of the upper Min River (Zhang

372 et al., 2005). **(d)** Hillslope angle and **(e)** local relief along the upper Min River. A 4*4

373 km grid was delineated along the upper Min River (~260 km). The highest ridgeline

374 and riverbed height in the grid were extracted from a DEM map, and the local relief

375 was then obtained by calculating the highest ridgeline minus the riverbed height. The

376 hillslope angle was obtained by solving for tan (local relief/slope length).

377   The EM_2 in segment IV reaches the highest value (185.8 μm, 67.4%) of the whole

sequence and corresponds to the 63–250 μm fraction (59.5%), which is consistent with previous studies shown that fluvial deposits are composed mainly of a medium-sand component (modal size: 200–400 μm) (Middleton, 1976; Tsoar and Pye, 1987; Bennett and Best, 1995; Dietze et al., 2014). In the C-M diagram, sample data that lie close to the C = M line reflect the suspension transport of riverbed sediments (Fig. 6a) (Passega, 1957; Singh et al., 2007). In addition, the single peak mode (Fig. S2d) of segment IV represents the river transport process and sedimentary environment (McKinney and Sanders, 1978), and the small range of the grain-size frequency distribution also reflects a well-sorted effect of fluvial transport (Sun et al., 2002). Therefore, the EM_2 mainly reflect typical fluvial sediments.

EM_3 corresponds to the coarsest grain-size components (>250 μm) and has the highest value (351.7 μm, 38.6%) of the whole sequence in segment III. The maximum values of C and M (Figs. 7a, b) in segment III indicate that it had the highest transport capacity (Passega, 1957; Singh et al., 2007; Bravard et al., 2014). Therefore, EM_3 represents the local sedimentary component transported over short distances (Dietze et al., 2014; Jiang et al., 2014, 2017). Samples from segment III are in the PQ section in C-M diagram (Fig. 6a), indicating dominant rolling and jumping transportation processes (Passega, 1957). Meanwhile, the SUS values in segment III increase abruptly near exposures of the Pengguan complex (28.5–546.5, mean 227.3), although lower SUS values occur in the surrounding area (e.g., Zagunao River: 9.1–114.1, mean 34.1, Fig. S4; Zipingpu reservoir: 5–60, Zhang et al., 2019; and segments I and II: 5.3–30.6, mean 11.5, Fig. 3). The precipitation in segment III is generally low (400–700 mm/a)

and only significantly increases near the Zipingpu reservoir (1200 mm/a), so that the

sedimentary changes muted until 2 years after the Wenchuan earthquake (Zhang et al.,

2019) (Fig. 1b). In addition, the mean grain size in segment III (170.2 μm) increases

before the Zagunao River (mean 83.1 μm, Fig. S4) joins the Min River (Fig. 1b. 3), so

contribution from the Zagunao River can be precluded. Therefore, the abnormally high

grain-size and SUS values in segment III are likely caused by a local provenance change.

Based on the indicative significance of EMs, combined with the regional climatic and

tectonic background, the main control mechanisms of river sediment variation in

different segments of the upper Min River are discussed below.

5.2 Climate controlled fine-grained fluvial sediments

The windy and semi-arid climate in the study area is responsible for more fine

particle components (EM_1) in segment I (Jiang et al., 2014), which caused EM_1 gradual

decrease downstream as the wind weakens (Fig. 5). The relatively low precipitation

(400–700 mm/a) and low runoff (18.4–43.4×10^8 m^3) (Fig. 1b) in segment I reflect the

limited transport capacity of the river, and the angular gravels on the riverbed also

indicate weak scouring, which preserves more fine-grained components (EM_1) in

fluvial sediments. Segment I developed along the Minjiang Fault (Fig. 1a), which has

a low slip rate (0.30–0.53 mm/a, Kirby et al., 2000; Zhou et al., 2000, 2006; Tan et al.,

2019) and therefore a weak influence on local provenance supply (Jiang et al., 2014,

2017). In addition, the wide riverbed (Fig. 2a), relatively low hillslope angle, and local

relief in the Minjiangyuan - Songpan segment (Figs. 7d, e) causes *in situ* retention of

locally sourced coarse components. Therefore, EM_2 and EM_3 make only a minor

422   contribution to the fluvial sediments in segment I.

423   Segment IV is located inside the Sichuan Basin and is completely unaffected by

424   alpine valleys in the eastern TP. It is characterized by a wide and flat geomorphological

425   surface (Fig. 2d). The significant downstream increase in precipitation and runoff in the

426   Zipingpu reservoir (Fig. 1b) indicates that fluvial action was the main control on

427   sediment transportation in segment IV. In addition, well-rounded pebbles (Fig. 2d) on

428   the riverbed prove this point.

429   **5.3 Coarse-grained deposits controlled by tectonism**

430   Fluvial sediments coarsen at the transition between segments I and II, highlighting

431   an increase in EM_2 and EM_3 content, and a higher M value (Figs. 3, 7). This locality

432   occurs at the intersection of the Minjiang Fault and the Songpinggou Fault (Fig. 1a),

433   which was the epicenter of the Diexi *Ms* 7.5 earthquake in 1933 (Chen et al., 1994; Ren

434   et al., 2018). As a result, the outcropping bedrock was severely damaged and so

435   provided new, fresh, and local sediment sources (EM_3). Downstream from Diexi, field

436   surveys exhibit that the altitude decreases by 400 m over a horizontal distance of 20 km,

437   such that the longitudinal slope of the riverbed (12.6‰, Fig. 7c, Zhang et al., 2005) and

438   the hillslope angle (41.4°, Fig. 7d) are highest in this region when compared to the entire

439   study area, which imply a higher regional denudation rate forced by active tectonics

440   (Zhang et al., 2005; Whittaker et al., 2007a). These remarkable changes of

441   geomorphology correspond well to a twofold increase in erosion coefficients that occur

442   within 15 km of major faults in the eastern TP (Kirkpatrick et al., 2020) and more

443   intense denudation at the location of seismogenic faulting along high-relief plateau

444   margins (Li et al., 2017). The narrow valley and direct contact between the riverbed and

445   hillside on either side in segment II (Fig. 2b) provide favorable conditions for rolling

446 and jumping transportation of sediment along the hillslope. In addition, the rapid rising

447 of the base-level of the Min River in segment II enhances the river's cutting and

448 transport capacity (Merritts and Vincent, 1989; Stokes et al., 2002; Cheng et al., 2004;

449 Whittaker et al., 2007a; Boulton et al., 2014).

450 EM$_3$ rapidly reaches its maximum fluctuation range in segment III (Fig. 5), likely

451 due to the maximum transport force (C value) in the area (Fig. 7). The regional

452 precipitation in segment III is low (400–700 mm/a) and only significantly increases

453 near the Zipingpu reservoir (1200 mm/a) (Fig. 1b). From a tectonic perspective, the

454 Maoxian-Wenchuan Fault, with a high dextral slip rate (1.0–3.8mm /a; Chen and Li,

455 2013; Wang et al., 2017) and vertical slip rate (~1–2 mm/a; Liu et al., 2015), mainly

456 controls the grain-size distribution of segment III (Fig.1). Previous studies have shown

457 that the Maoxian - Wenchuan Fault occurs at a band of maximum exhumation along the

458 eastern Longmen Shan Fault zone since the late Miocene (Tan et al., 2019). Therefore,

459 rapid regional uplift and denudation rates (Kirby et al., 2002; Liang et al., 2013) not

460 only generated a larger hillslope angle (mean value of 24.9°) and the highest local relief

461 (2188 m), but also provided widespread source of fresh, coarse-grained, and local

462 sediment (Whittaker et al., 2007b, 2010) in segment III. At the beginning of segment

463 III, the river sediments become significantly coarser, indicating a transient response to

464 the tectonics, manifested by a large amount of material output (Whittaker et al., 2010).

465 Moreover, the PQ distribution of segment III in the calculated C-M diagram (Fig. 4)

466 shows the importance of rolling and jumping transport mechanisms (Passega, 1957),

467 which correlate with the steep landform features in segment III (Fig. 2c). Exposures of

468 hard Mesozoic granites instantaneously provide a local source of coarse components,

and thus correspond to the maximum M and C values. Although regional climate generally has a weak influence on the supply of coarse particles, the concentrated distribution of particles within the calculated grain-size frequency distribution (Fig. S2c) indicates that fluvial action played an effective role in sorting local sediment sources (Sahu, 1964; Sun et al.,2002; Frings, 2008). The persistent occurrence of the coarsest grain-size across the segment III responds to the fact that the catchments crossing faults maintain their high slip rate over time, which exhibits a sharp contrast to that of segment I.

Generally, a large earthquake is followed by a period of enhanced mass wasting and fluvial sediment evacuation (Hovius et al., 2011; Wang et al., 2015). The Wenchuan M_s 8.0 earthquake in 2008 caused severe geomorphological damage in this region, and the annual average suspended sediment flow in regional rivers increased by a factor of 3–7 following the earthquake. The river recovered to its pre-earthquake level just 1.2 ± 0.9 years later (Wang et al., 2015). However, over 70% of the co-seismic debris has stabilized in place along the hillslopes during the following decades (Dai et al., 2021) and will take 370 years to be removed out of the mountains (Wang et al., 2017). The above results are sufficient to show that the extensive existence of gravel in Min River can reveal tectonic activity for a long time. However, these studies cannot explain the relatively fine fluvial and wind transport characteristics. In addition, we believe that co-seismic debris generated by the Wenchuan earthquake in 2008 had negligible influence on our sample collection campaign conducted in 2017.

5.4 Geomorphic morphology reveals tectonic activity

Alpine valleys characterize the landscape of the upper reaches of the Min River in the eastern TP (Figs. 2, 7) and have an incision depth of 300–1500 m (Li et al., 2005; Zhang et al., 2005) (Fig. 6a). In segment I, hillslope angles and local relief gradually increase downstream along the Minjiang Fault from 5° to 34.8° and 243 m to 1572 m, respectively (Fig. 7d, e). However, these changes seem to be decoupled with the high and stable proportion of fine-grained background dust in the fluvial sediments of segment I (Figs. 3, 5), which is an open and interesting question. The consistent precipitation and runoff rates explain the calculated consistency in transport power, as defined by unchanging values of C and M (Fig. 7). We note that the longitudinal slope of the riverbed (6.7–7.6‰, Fig. 7c; Zhang et al., 2005) in segment I steadily changes as altitude decreases from 3460 m to 2190 m; therefore, gradual steepening of the landscape is likely a response to enhanced river-related erosion (Merritts and Vincent, 1989; Stokes et al., 2002; Cheng et al., 2004). The high vegetation density in the Minjiangyuan - Songpan region is also probably modulated by the lower topographic slope (Figs. 2a, 7) (Olen et al., 2016). These are consistent with generally weak activity of the Minjiang Fault (Kirby et al., 2000; Zhou et al., 2000, 2006; Tan et al., 2019).

In segment II, the hillslope angle (12.3–41.4°, with a mean of 30.1°) is generally steeper than the average for the whole study area (25.1°), and the highest angles (41.4°) far exceed the stability threshold of ~32° for landslide denudation, which suggests that landslide-dominated hillslope denudation has kept pace with the rates of rock uplift and valley incision in segment II (Burbank, et al., 1996; Montgomery and Brandon, 2002; Clarke and Burbank, 2010; Wang et al., 2014). Along the studied transect, local relief

in segment II initially increases and then decreases (Fig. 7c), and the flow direction of

the Min River also changes from roughly N-S to NW-SE (Fig. 1a). The lithology in

segment II changes from Triassic to Silurian (Fig. 1a), and seismic activity transitions

from the Minjiang Fault to the Maoxian - Wenchuan Fault. Given that segment II

records the lowest annual rainfall in the study area (<500 mm/a, Fig. 1), this

transformation of tectonic activity and lithology likely plays a dominant role on fluvial

erodibility (Selby, 1980; Stokes et al., 2008; Whittaker et al., 2007a; Zondervan et al.,

2020), and influences changes of regional geomorphology and river drainage.

Hillslope angles (14.9°–34.3°, mean 24.9°) and local relief (689–2188 m, mean

1463 m) in segment III exhibit a general increase along the Maoxian - Wenchuan Fault

(Figs. 1, 7), although they differ from the increasing trends shown in segment I. For

example, the highest local relief throughout the entire sequence occurs in segment III,

although its mean hillslope angle (24.9°) is lower than the mean value (25.1°) of the

entire sequence (Fig. 7). In addition, precipitation and runoff only show a significant

increase adjacent to the Zipingpu reservoir (Fig. 1). We note that the regional bedrock

in segment III is hard Mesozoic granites of the Pengguan complex (Fig. 1a), and that

the Maoxian-Wenchuan Fault is situated on the zone of maximum exhumation along

the Longmen Shan fault zone (Tan et al., 2019). Therefore, the higher local relief along

segment III indicates that active Maoxian-Wenchuan Fault (Tan et al., 2019) caused

enhanced rock uplift and valley incision (Whittaker et al., 2007a; Tan et al., 2019),

which accounts for the largest transport forces (C values, Fig. 7) and the coarsest local

components (EM$_3$, Fig. 5) in this section. Nevertheless, a decrease in the mean hillslope

angle within segment III may be attributed to hardening of the exposed bedrock of the Pengguan complex rather than weakening of tectonic activity along the Maoxian-Wenchuan Fault. Even if the shortening rates are generally slow in the eastern TP (Densmore et al., 2008; Zhang, 2013), and satellite data may be equivocal (Kirby et al., 2008), grain-size analysis of fluvial sediments combined with topographic analyses can help guide the identification of regional tectonic activity effectively (Kirby et al., 2003, 2008; Schoenbohm et al., 2004; Tan et al., 2019).

6 Conclusion

Grain-size analysis was conducted on modern fluvial sediments of the upper Min River to extract regional tectonic signals in the eastern TP. Integrated with vegetation, hydrology, geomorphology (local relief and hillslope) and geology (fault and lithology) data, three segments of tectonic activity along the upper Min River were identified. The Minjiang Fault, situated in the Minjiangyuan - Diexi segment, generally shows weak tectonic activity. The Maoxian-Wenchuan Fault from Diexi - Wenchuan to Wenchuan - Dujiangyan segments shows enhanced tectonic activity. However, the segment from Dujiangyan to the Sichuan Basin records almost no evidence of tectonic activity.

In this study, we report a new approach that can reveal the regional tectonic activity by analyzing fluvial sediments collected from tectonically active regions. The novelty of this research method and the reliability of the results provide a key framework with which regional tectonic activity can be revealed through the study of fluvial sediments in other tectonically active localities worldwide.

Data availability

Data are available in the figshare database (https://doi.pangaea.de/10.6084/m9.figshare.17111402).

Author contributions

The paper was written by WS and HCJ with major contributions by HYX. SYM got geomorphic data. WS, HYX and SQZ participated in field surveys and sample collection. SQZ, JWF and XTW conducted laboratory tests and interpreted the results. All authors reviewed and approved the paper.

Competing interests

The contact author has declared that neither they nor their co-authors have any competing interests.

Acknowledgements

This study was supported by the National Nonprofit Fundamental Research Grant of China, Institute of Geology, China Earthquake Administration (IGCEA2126 and IGCEA1906) and the Grant of the State Key Laboratory of Earthquake Dynamics, Institute of Geology, China Earthquake Administration (LED2022A06).

References

Beek, V.D., Bishop, P.: Cenozoic river profile development in the upper Lachlan catchment (SE Australia) as a test of quantitative fluvial incision models. J. Geophys. Res. Solid Earth, 108(B6), 2309, https://doi.org/10.1029/2002JB002125, 2003.

Bennett, S.J., Best, J.L.: Mean flow and turbulence structure over fixed, two-dimensional dunes: implications for sediment transport and bedform stability. Sedimentology, 42(3), 491-513, https://doi.org/10.1111/j.1365-3091.1995.tb00386.x, 1995.

Blanckenburg, F.: The control mechanisms of erosion and weathering at basin scale from cosmgoenic nuclides in river sediment. Earth Planet. Sci. Lett., 237, 462-479, https://doi.org/10.1016/j.epsl.2005.06.030, 2005.

Boulton, S.J., Stokes, M., Mather, A.E.: Transient fluvial incision as an indicator of active faulting and Plio-Quaternary uplift of the Moroccan High Atlas. Tectonophysics, 633(1), 16-33, https://doi.org/10.1016/j.tecto.2014.06.032, 2014.

Bravard, J.P., Goichot, M., Tronchère, H.: An assessment of sediment-transport processes in the Lower Mekong River based on deposit grain sizes, the CM technique and flow-energy data. Geomorphology, 207, 174-189, https://doi.org/10.1016/j.geomorph.2013.11.004, 2014.

Burbank, D. W., Blythe, A. E., Putkonen, J., Pratt-Sitaula, B., Gabet, E., Oskin, M., Barros, A., Ojha, T. P.: Decoupling of erosion and precipitation in the Himalayas. Nature, 426(6967), 652-655, https://doi.org/doi:10.1038/nature02187, 2003.

Burbank, D.W., Fielding, E., Anderson, R.S., Brozovic, N., Reid, M. D.C., Leland, J.: Bedrock incision, rock uplift and threshold hillslopes in the northwestern Himalayas. Nature, 379(6565), 505-510, https://doi.org/10.1038/379505a0, 1996.

Chen, H., Li, Y.: Water system responding to the dextral strike-slipping of the Longmen Shan fault zone in the upper Min River basin. J. Mount. Sci., 31(2), 211-217, https://doi.org/10.3969/j.issn.1008-2786.2013.02.010, 2013 (in Chinese).

Chen, S.A., Michaelides, K., Grieve, S.W.D., Singer, M.B.: Aridity is expressed in river topography globally. Nature, 573, 573-577, https://doi.org/10.1038/s41586-019-1558-8, 2019.

Chen, S.F., Wilson, C., Deng, Q.D., Zhao, X.L. Zhi, L.L.: Active faulting and block movement associated with large earthquakes in the Min Shan and Longmen Mountains, northeastern Tibetan Plateau. J. Geophys. Res. Solid Earth, 99(B12), 24025-24038,

https://doi.org/10.1029/94JB02132, 1994.

Chen, Z., Burchfiel, B.C., Liu, Y., King, R.W., Royden, L.H., Tang, W., Wang, E., Zhao, J., Zhang, X.: Global positioning system measurements from eastern Tibet and their implications for India/Eurasia intercontinental deformation. J. Geophys. Res. Solid Earth, 105(B7), 16215-16227, https://doi.org/10.1029/2000jb900092, 2000.

Cheng, S.P., Deng, Q.D., Li, C.Y., Yang, G.Z.: Dynamical mechanism, physical erosion processes and influence factors of fluvial incision: A review and prospect. Quat. Sci., 24, 421-429, https://doi.org/10.3321/j.issn:1001-7410.2004.04.008, 2004 (in Chinese).

Clapp, E.M., Bierman, P.R., Caffee, M.: Using ^{10}Be and ^{26}Al to determine sediment generation rates and identify sediment source areas in an arid region drainage basin. Geomorphology, 45, 89-104, https://doi.org/10.1016/S0169-555X(01)00191-X, 2002.

Clapp, E.M., Bierman, P.R., Schick, A.P., Lekach, J., Enzel, Y., Caffee, M.: Sediment yield exceeds sediment production in arid region drainage basins, Geology, 28, 995-998, https://doi.org/10.1130/0091-7613(2000)28<995:SYESPI>2.0.CO;2, 2000.

Clarke, B.A., Burbank, D.W.: Bedrock fracturing, threshold hillslopes, and limits to the magnitude of bedrock landslides. Earth Planet. Sci. Lett., 297(3-4), 577-586, https://doi.org/10.1016/j.epsl.2010.07.011, 2010.

Dai, F.C., Xu, C., Yao, X., Xu, L., Tu, X.B., Gong, Q.M.: Spatial distribution of landslides triggered by the 2008 Ms 8.0 Wenchuan earthquake, China. J. Asian Earth Sci., 40, 883-895, https://doi.org/10.1016/j.jseaes.2010.04.010, 2011.

Dai, L.X., Scaringi, G., Fan, X.M., Yunus, A.P., Liu, Z.J., Xu, Q., Huang, R.Q.: Coseismic debris remains in the orogen despite a decade of enhanced landsliding. Geophys. Res. Lett., https://doi.org/10.1029/2021GL095850, 2021.

Deng, Q.D., Cheng, S.P., Ma, J., Du, P.: Seismic activities and earthquake potential in the Tibetan Plateau. Chinese J. Geophys., 57(5), 2025-2042, https://doi.org/10.1002/cjg2.20133, 2014 (in Chinese).

Densmore, A. L., Ellis, M.A., Yong, L., Zhou, R., Richardson, N.: Active tectonics of the Beichuan and Pengguan faults at the eastern margin of the Tibetan Plateau. Tectonics, 26(4), TC4005, https://doi.org/10.1029/2006TC001987, 2008.

Duvall, A., Kirby, E., Burbank, D.: Tectonic and lithologic controls on bedrock channel profiles and processes in coastal California. J. Geophys. Res. Earth Surface, 109, F03002,

https://doi.org/10.1029/2003JF000086, 2004.

Dietze, E., Maussion, F., Ahlborn, M., Diekmann, B., Hartmann, K., Henkel, K., Kasper, T., Lockot, G., Opitz, S., Haberzettl, T.: Sediment transport processes across the Tibetan Plateau inferred from robust grain-size end members in lake sediments. Clim. Past, 10, 91-106, https://doi.org/10.5194/cp-10-91-2014, 2014.

Ding, H.R., Ma, G.W., Ni, S.J., Shi, Z.M., Zhao, G.H., Yan, L., Yan, Z.K.: Study on sediment discharge increase caused by Wenchuan earthquake landslide and heavy rainfall in the upper reaches of the Min River. J. Sichuan Univ., 46(3), 49-55, https://doi.org/10.15961/j.jsuese.2014.03.006, 2014 (in Chinese).

Egli, R.: Analysis of the field dependence of remanent magnetization curves. J. Geophys. Res. Solid Earth, 108(B2), 1-26, https://doi.org/10.1029/2002JB002023, 2003.

Frings, R.M.: Downstream fining in large sand-bed rivers. Earth Sci. Rev., 87, 39-60, https://doi.org/10.1016/j.earscirev.2007.10.001, 2008.

Hovius, N., Meunier, P., Lin, C.W., Chen, H., Chen, Y.G., Dadson, S., Horng, M.J., Lines, M.: Prolonged seismically induced erosion and the mass balance of a large earthquake. Earth Planet. Sci. Lett., 304(3-4), 347-355, https://doi.org/10.1016/j.epsl.2011.02.005, 2011.

Jiang, H., Zhang, J., Zhang, S., Zhong, N., Wan, S., Alsop, G.I., Xu, H., Guo, Q., Yan, Z.: Tectonic and climatic impacts on environmental evolution in East Asia during the Palaeogene. Geophys. Res. Lett., 49, e2021GL096832, https://doi.org/10.1029/2021GL096832, 2022.

Jiang, H.C., Shevenell, A., Yu, S., Xu, H.Y., Mao, X.: Decadal- to centennial-scale East Asian summer monsoon variability during the Medieval Climate Anomaly reconstructed from an eastern Tibet lacustrine sequence. J. Paleolimnology, 54, 205-222, https://doi.org/10.1007/s10933-015-9847-1, 2015.

Jiang, H.C., Mao, X., Xu, H.Y., Yang, H.L., Ma, X.L., Zhong, N., Li, Y.H.: Provenance and earthquake signature of the last deglacial Xinmocun lacustrine sediments at Diexi, East Tibet. Geomorphology, 204, 518-531, https://doi.org/10.1016/j.geomorph.2013.08.032, 2014.

Jiang, H.C., Zhong, N., Li, Y.H., Ma, X.L., Xu, H.Y., Shi, W., Zhang, S.Q., Nie, G.Z.: A continuous 13.3-ka record of seismogenic dust events in lacustrine sediments in the eastern Tibetan Plateau. Sci. Rep., 7:15686, https://doi.org/10.1038/s41598-017-16027-8, 2017.

Jiang, H.C., Zhong, N., Li, Y.H., Xu, H.Y., Yang, H.L., Peng, X.P.: Soft sediment deformation structures in the Lixian lacustrine sediments, Eastern Tibetan Plateau and implications for

postglacial seismic activity. Sediment. Geol., 344, 123-134, https://doi.org/10.1016/j.sedgeo.2016.06.011, 2016.

Kirby, E., Whipple, K.X., Burchfiel, B.C., Tang, W.Q., Berger, G., Sun, Z.M., Chen, Z.L.: Neotectonics of the Min Shan, China: implications for mechanisms driving quaternary deformation along the eastern margin of the Tibetan Plateau. GSA Bull., 112(3), 375-393, https://doi.org/10.1130/0016-7606(2000)112<375:NOTMSC>2.0.CO;2, 2000.

Kirby, E., Reiners, P.W., Krol, M.A., Whipple, K.X., Hodges, K.V., Farley, K.A., Tang, W.Q., Chen, Z.L.: Late Cenozoic evolution of the eastern margin of the Tibetan Plateau: inferences from 40Ar/39Ar and, U-Th/He thermochronology. Tectonics, 21(1), 1-20, https://doi.org/10.1029/2000TC001246, 2002.

Kirby, E., Whipple, K. and Harkins, N.: Topography reveals seismic hazard. Nat. Geosci., 1(8), 485-487, https://doi.org/10.1038/ngeo265, 2008.

Kirby, E., Whipple, K.X., Tang, W.Q. and Chen, Z.L.: Distribution of active rock uplift along the eastern margin of the Tibetan Plateau: Inferences from bedrock channel longitudinal profiles. J. Geophys. Res. Solid Earth, 108(B4), 2217, https://doi.org/doi:10.1029/2001JB000861, 2003.

Kirkpatrick, H.M., Moon, S., Yin, A., Harrison, T.M.: Impact of fault damage on eastern Tibet topography. Geology, 48, https://doi.org/10.1130/G48179.1, 2020.

Li, G., Westa, A.J., Densmoreb, A.L., Jin, Z.D., Zhang. F., Wang, J., Clark, M., Hilton, R.G.: Earthquakes drive focused denudation along a tectonically active mountain front. Earth Planet. Sci. Lett., 472, 253-265, https://doi.org/10.1016/j.epsl.2017.04.040, 2017.

Li, Y., Cao, S.Y., Zhou, R.J., Densmore, A.L., Ellis, M.: Late Cenozoic Minjiang incision rate and its constraint on the uplift of the eastern margin of the Tibetan plateau. Acta Geol. Sinica, 79(1), 28-37, https://doi.org/10.3321/j.issn:0001-5717.2005.01.004, 2005 (in Chinese).

Li, Y.H., Jiang, H.C., Xu, H.Y., Liang, L.J.: Analyses on the triggering facrors of large quantities of landslides in the upper reaches of the Minjiang River, Sichuan province. Seism. Geol., 37(4), 1147-1161, https://doi.org/10.3969/j.issn.0253-4967.2015.04.017, 2015 (in Chinese).

Liang, S.M., Gan, W.J., Shen, C.Z., Xiao, G.R., Liu, J., Chen, W.T., Ding, X.G., Zhou, D.M.: Three-dimensional velocity field of present-day crustal motion of the Tibetan Plateau derived from GPS measurements. J. Geophys. Res. Solid Earth, 118(10), 1-11, https://doi.org/10.1002/2013JB010503, 2013.

Liang, L.J. and Jiang, H.C.: Geochemical composition of the last deglacial lacustrine sediments in

East Tibet and implications for provenance, weathering and earthquake events. Quat. Inter., 430, 41-51, https://doi.org/10.1016/j.quaint.2015.07.037, 2017.

Liu, M.: Research on the risk stone under wind loading with wind tunnel test in the Min River Valley. Chengdu University of Technology, Sichuan, p. 10-38, 2014 (in Chinese).

Lin, M.B.: The huge Wenchuan earthquake and Longmen tectonic belt. J. Chengdu Univ. Technol., 35(4), 366-370, https://doi.org/10.3969/j.issn.1671-9727.2008.04.004, 2008 (in Chinese).

Liu, W.M., Yang, S.L., Fang, X.M.: Loess recorded climatic change during the last glaciation on the eastern Tibetan Plateau, western Sichuan. J. Jilin Univ. Earth Sci. Edi., 43(3), 974-982, https://doi.org/http://ir.itpcas.ac.cn/handle/131C11/2852, 2013 (in Chinese).

Liu, X.X., Wu, Y.Q., Jiang, Z.S., Zhan, W., Li, Q., Wen, W.X., Zhou, Z.Y.: Preseismic deformation in the seismogenic zone of the Lushan Ms 7.0 earthquake detected by GPS observations. Sci. China, Earth Sci., 45(9), 1198-1207, https://doi.org/10.1007/s11430-015-5128-0, 2015.

Lu, H.Y., An, Z.S.: Comparison of grain-size distribution of Red Clay and Loess-paleosol deposits in Chinese Loess Plateau. Acta Sediment. Sinica, 17(2), 226-232, https://doi.org/10.3969/j.issn.1000-0550.1999.02.011, 1999.

Ma, K.M., Fu, B.J., Liu, S.L., Guan, W.B., Liu, G.H., Lu, Y.H., Anand, M.: Multiple-scale soil moisture distribution and its implications to ecosystem restoration in an arid river valley, China. Land Degrad. Develop., 15(1), 75-85, https://doi.org/10.1002/ldr.584, 2004.

Ma, Y.W., Wang, G.Z., Hu, X.W.: Tectonic deformation of Pengguan complex as a nappe. Acta Geol. Sichuan, 2, 110-114, 1996 (in Chinese).

Matmon, A., Bierman, P.R., Larsen, J., Southworth, S., Pavich, M., Caffee, M.: Temporally and spatially uniform rates of erosion in the southern Appalachian Great Smoky Mountains. Geology, 31, 155-158, https://doi.org/10.1130/0091-7613(2003)0312.0.CO;2, 2003a.

Matmon, A., Bierman, P.R., Larsen, J., Southworth, S., Pavich, M., Finkel, R., Caffee, M.: Erosion of an ancient mountain range, the Great Smoky Mountains, North Carolina and Tennessee. Amer. J. Sci., 303, 817-855, https://doi.org/10.2475/ajs.303.9.817, 2003b.

McKinney, G.M., Sanders, J.E.: Principles of sedimentology. Wiley, New York, No. of pages 792, 1978.

Merritts, D., Vincent, K.R.: Geomorphic response of coastal streams to low, intermediate, and high rates of uplift, Medocino triple junction region, northern California. GSA Bull., 101, 1373-

1388, https://doi.org/10.1130/0016-7606(1989101<1373:GROCST>2.3.CO;2, 1989.

Middleton, G.V.: Hydraulic interpretation of sand size distributions. J. Geol., 84(4), 405-426, https://doi.org/10.1086/628208, 1976.

Molnar, P., Anderson, R.S., Anderson, S.P.: Tectonics, fracturing of rock, and erosion. J. Geophys. Res. Earth Surface, 112, F03014, https://doi.org/10.1029/2005JF000433, 2007.

Montgomery, D.R., Brandon, M. T.: Topographic controls on erosion rates in tectonically active mountain ranges. Earth Planet. Sci. Lett., 201(3), 481-489, https://doi.org/10.1016/S0012-821X(0200725-2, 2002.

Najman, Y.: The detrital record of orogenesis: A review of approaches and techniques used in the Himalayan sedimentary basins. Earth Sci. Rev., 74(1-2), 1-72, https://doi.org/10.1016/j.earscirev.2005.04.004, 2006.

Nichols, K.K., Bierman, P.R., Caffee, M., Finkel, R., Larsen, J.: Cosmogenically enabled sediment budgeting. Geology, 33(2), 133-136, https://doi.org/10.1130/g21006.1, 2005.

Olen, S.M., Bookhagen, B., Strecker, M.R.: Role of climate and vegetation density in modulating denudation rates in the Himalaya. Earth Planet. Sci. Lett., 445, 57-67, https://doi.org/10.1016/j.epsl.2016.03.047, 2016.

Owen, L.A.: Tectonic geomorphology: a perspective. In: Shroder, J. (Editor in Chief), Owen, L.A. (Ed.), Treatise on Geomorphology. Academic Press, San Diego, CA, vol. 5, Tectonic Geomorphology, pp. 3-12, 2013.

Passega, R.: Texture as characteristic of clastic deposition. Bull. Amer. Assoc. Petrol. Geol., 41, 1952-1984, https://doi.org/10.1306/0BDA594E-16BD-11D7-8645000102C1865D, 1957.

Paterson, G.A., Heslop, D.: New methods for unmixing sediment grain size data. Geochem. Geophys. Geosyst., 16(12), 4494-4506, https://doi.org/info:doi/10.1002/2015GC006070, 2015.

Perg, L.A., Anderson, R.S., Finkel, R.C.: Use of cosmogenic radionuclides as a sediment tracer in the Santa Cruz littoral cell, California, USA. Geology, 31, 299-302, https://doi.org/10.1130/0091-7613(2003)031<0299:UOCRAA>2.0.CO;2, 2003.

Ren, J.J., Xu, X.W., Zhang, S.M., Yeats, R. S., Chen, J.W., Zhu, A.L., Liu, S.: Surface rupture of the 1933 Ms 7.5 Diexi earthquake in eastern Tibet: implications for seismogenic tectonics. Geophys. J. Inter., 212(3), 627-1644, https://doi.org/10.1093/gji/ggx498, 2018.

Riebe, C.S., Kirchner, J.W., Granger, D.E., Finkel, R.C.: Erosional equilibrium and disequilibrium in the Sierra Nevada, inferred from cosmogenic ^{26}Al and ^{10}Be in alluvial sediment. Geology, 28, 803-806, https://doi.org/10.1130/0091-7613(2000)282.0.CO;2, 2000.

Riebe, S.R., Kirchner, J.W., Granger, D.E., Finkel, R.C.: Strong tectonic and weak climatic control of long-term chemical weathering rates. Geology, 29, 511-514, https://doi.org/10.1130/0091-7613(2001)0292.0.CO;2, 2001.

Sahu, B. K.: Depositional mechanisms from the size analysis of clastic sediments. J. Sediment. Res., 34, 73-83, https://doi.org/10.1306/74D70FCE-2B21-11D7-8648000102C1865D, 1964.

Schoenbohm, L.M., Whipple, K.X., Burchfiel, B.C., Chen, L.: Geomorphic constraints on surface uplift, exhumation, and plateau growth in the Red River region, Yunnan Province, China. GAS Bull., 116, 895-909, https://doi.org/10.1130/B25364.1, 2004.

Schumm, S.A., Khan, H.R.: Experimental study of channel patterns. Nature, 233(5319), 407-9, https://doi.org/10.1038/233407a0, 1971.

Schumm, S.A., Khan, H.R.: Experimental study of channel patterns. GAS Bull., 83(6), 1755-1770, https://doi.org/10.1130/0016-7606(1972)83[1755:ESOCP]2.0.CO;2, 1972.

Selby, M.J.: A rock mass strength classification for geomorphic purposes, with tests from Antarctica and New Zealand: Zeitschrift für Geomorphologie, v. 24, p. 31–51, 1980.

Shen, Y.Q., Guo, C.B., Wu, R.A., Ren, S.S., Su, F.R., Zhang, T.: Analysis on the development characteristics and engineering geomechanical properties of the Songpan loess, western Sichuan province, China. J. Geomech., 23(5), 131-142, https://doi.org/10.3969/j.issn.1006-6616.2017.05.013, 2017 (in Chinese).

Shi, W., Jiang, H.C., Mao, X., Xu, H.Y.: Pollen record of climate change during the last deglaciation from the eastern Tibetan Plateau. PLOS ONE, 15(5), e0232803, https://doi.org/10.1371/journal.pone.0232803, 2020.

Shi, W., Jiang, H.C., Alsop, G.I., Wu, G.: A Continuous 13.3-Ka paleoseismic record constrains major earthquake recurrence in the Longmen Shan collision zone. Front. Earth Sci., 10:838299, https://doi.org/10.3389/feart.2022.838299, 2022.

Singh, M., Singh, I.B., Müller, G.: Sediment characteristics and transportation dynamics of the Ganga River. Geomorphology, 86(1/2), 144-175, https://doi.org/10.1016/j.geomorph.2006.08.011, 2007.

Snyder, N., Whipple, K., Tucker, G., Merritts, D.: Landscape response to tectonic forcing: digital elevation model analysis of stream profiles in the Mendocino triple junction region, northern California. GAS Bull., 112, 1250-1263, https://doi.org/10.1130/0016-7606(2000)112<1250:LRTTFD>2.0.CO;2, 2000.

Snyder, N.P. and Whipple, K.X.: Importance of a stochastic distribution of floods and erosion thresholds in the bedrock river incision problem. J. Geophys. Res. Solid Earth, 108, 2117, https://doi.org/10.1029/2001JB001655, 2003.

Stock, J. D., Dietrich, W. E.: Valley incision by debris flows: evidence of a topographic signature. Water Resour. Res., 39(4), ESG 1-1, https://doi.org/10.1029/2001WR001057, 2003.

Stokes, M., Mather, A.E., Belfoul, A., Farik, F.: Active and passive tectonic controls for transverse drainage and river gorge development in a collisional mountain belt (Dades Gorges, High Atlas Mountains, Morocco). Geomorphology, 102(1), 2-20, https://doi.org/10.1016/j.geomorph.2007.06.015, 2008.

Stokes, M., Mather, A.E., Harvey, A.M.: Quantification of river-capture-induced base-level changes and landscape development, Sorbas Basin, SE Spain. Geol. Soc. London Spec. Publ., 191(1), 23-35, https://doi.org/10.1144/GSL.SP.2002.191.01.03, 2002.

Sun, D.H., Bloemendal, J., Rea, D.K., An, Z.S., Vandenberghe, J., Lu, H.Y., Sun, R.X., Liu, T.S.: Bimodal grain-size distribution of Chinese loess, and its palaeoclimatic implications. Catena, 55(3), 325-340, https://doi.org/10.1016/S0341-8162(0300109-7, 2004.

Sun, D.H., Bloemendal, J., Rea, D.K., Vandenberghe, J., Jiang, F.C., An, Z.S., Su, R.X.: Grain-size distribution function of polymodal sediments in hydraulic and aeolian environments, and numerical partitioning of the sedimentary components. Sediment. Geol., 152(3-4), 263-277, https://doi.org/10.1016/S0037-0738(0200082-9, 2002.

Sun, J.M, Li, S.H., Muhs, D. R., Li, B.: Loess sedimentation in Tibet: provenance, processes, and link with Quaternary glaciations, Quat. Sci. Rev., 26(17-18), 2265-2280, https://doi.org/10.1016/j.quascirev.2007.05.003, 2007.

Tan, X.B., Liu, Y.D., Lee, Y.H., Lu, R.Q., Xu, X.W., Suppe, J., Shi, F., Xu, C.: Parallelism between the maximum exhumation belt and the Moho ramp along the eastern Tibetan Plateau margin: Coincidence or consequence?. Earth Planet. Sci. Lett., 507, 73-84,

https://doi.org/10.1016/j.epsl.2018.12.001, 2019.

Tsoar, H., Pye, K.: Dust transport and the question of desert loess formation. Sedimentology, 34(1), 139-153, https://doi.org/10.1111/j.1365-3091.1987.tb00566.x, 1987.

Vandenberghe, J.: Grain size of fine-grained windblown sediment: a powerful proxy for process identification. Earth Sci. Rev., 121, 18-30, https://doi.org/10.1016/j.earscirev.2013.03.001, 2013.

Wang, J., Jin, Z.D., Hilton, R.G., Zhang, F., Densmore, A.L., Li, G., West A.J.: Controls on fluvial evacuation of sediment from earthquake-triggered landslides. Geology, 43(2), 115-118, https://doi.org/10.1130/G36157.1, 2015.

Wang, P., Zhang, B., Qiu, W.L., Wang, J.C.: Soft-sediment deformation structures from the Diexi paleo-dammed lakes in the upper reaches of the Minjiang River, east Tibet. J. Asian Earth Sci., 40(4), 865-872, https://doi.org/10.1016/j.jseaes.2010.04.006, 2011.

Wang, P., Scherler, D., Liu-Zeng, J., Mey, J., Avouac, J.P., Zhang, Y., Shi, D.: Tectonic control of Yarlung Tsangpo gorge revealed by a buried canyon in southern Tibet. Science, 346, 978-981, https://doi.org/10.1126/science.1259041, 2014.

Wang, W., Godard, V., Liu-Zeng, J., Scherler, D., Xu, C., Zhang, J.Y., Xie, K.J., Bellier, O., Ansberque, C., Sigoyer, J., Team, A.: Perturbation of fluvial sediment fluxes following the 2008 Wenchuan earthquake. Earth Surf. Process Land., 42(15), 2611-2622, https://doi.org/10.1002/esp.4210, 2017.

Wang, W., Godard, V., Liu-Zeng, J., Zhang, J.Y., Li, Z.G., Xu, S., Yao, W.Q., Yuan, Z.D., Aumaître, G., Bourlès, D.L., Keddadouche, K.: Tectonic controls on surface erosion rates in the Longmen Shan, eastern Tibet. Tectonics, 40(3), https://doi.org/10.1029/2020TC006445, 2021.

Wang, X.G., Li, C.Y., Lu, L.X., Dong, J.B.: Analysis of the late Quaternary activity along the Wenchuan-Maoxian fault-middle of the back- range fault at the Longmen Shan fault zone. Seism. Geol., 39(3), 572-586, https://doi.org/10.3969/j.issn.0253-4967.2017.03.010, 2017.

Weltje, G.L.: End-member modeling of compositional data: Numerical-statistical algorithms for solving the explicit mixing problem. Mathemat. Geol., 29(4), 503-549, https://doi.org/10.1007/BF02775085, 1997.

Wei, X.T., Jiang, H.C., Xu, H.Y., Fan, J.W., Shi, W., Guo, Q.Q., Zhang, S.Q.: Response of

sedimentary and pollen records to the 1933 Diexi earthquake on the eastern Tibetan Plateau. Ecol. Indicators, 129, 107887, https://doi.org/10.1016/j.ecolind.2021.107887, 2021.

Whipple, K.X.: Bedrock rivers and the geomorphology of active orogens. Ann. Rev. Earth Planet. Sci., 32, 151-185, https://doi.org/10.1146/annurev.earth.32.101802.120356, 2004.

Whittaker, A.C., Attalw, M., Allenn, P.A.: Characterising the origin, nature and fate of sediment exported from catchments perturbed by active tectonics. Basin Res., 22, 809-828, https://doi.org/10.1111/j.1365-2117.2009.00447.x, 2010.

Whittaker, A. C., Cowie, P.A., Attal, M., Tucker, G. E., Roberts, G.P.: Contrasting transient and steady-state rivers crossing active normal faults: new field observations from the central Apennines, Italy. Basin Res., 19(4), 529-556, https://doi.org/10.1111/j.1365-2117.2007.00337, 2007.

Wu, H.B., Liu, X.M., Lv, B., Ma, M.M., Ji, J.P., Wang, W.Y., Zhang, Y.Y., Hou, J.L.: Aeolian origin of the Twelve Apostles section, in Australia. Quat. Sci., 37(1), 82-96, https://doi.org/10.11928/j.issn.1001-7410.2017.01.08, 2017 (in Chinese).

Wobus, C., Heimsath, A., Whipple, K. Hodges, K.: Active out-of-sequence thrust faulting in the central Nepalese Himalaya. Nature, 434, 1008-1011, https://doi.org/10.1038/nature03499, 2005.

Wobus, C.W., Tucker, G.E., and Anderson, R.S.: Does climate change create distinctive patterns of landscape incision? J. Geophys. Res., 115, F04008, https://doi.org/10.1029/2009JF001562, 2010.

Xu, C., Xu, X.W., Dai, F.C., Xiao, J.Z., Tan, X.B., Yuan, R.M.: Landslides hazard mapping using GIS and weight of evidence model in Qingshui River watershed of 2008 Wenchuan earthquake struck region. J. Earth Sci., 23(1), 97-120, https://doi.org/10.1007/s12583-012-0236-7, 2012.

Xu, C., Xu, X.W., Yao, X., Dai, F.C.: Three, nearly complete inventories of landslides triggered by the May 12, 2008 Wenchuan Mw 7.9 earthquake of China and their spatial distribution statistical analysis. Landslides, 11(3), 441-461, https://doi.org/10.1007/s10346-013-0404-6, 2014.

Xu, H.Y., Jiang, H.C., Liu, K., Zhong, N.: Potential pollen evidence for the 1933 M7.5 Diexi earthquake and implications for post-seismic landscape recovery. Enviro. Res. Lett., 15:094043,

https://doi.org/10.1088/1748-9326/ab9af6, 2020.

Xu, H.Y., Jiang, H.C., Yu, S., Yang, H.L., Chen, J.: OSL and pollen concentrate 14C dating of dammed lake sediments at Maoxian, east Tibet, and implications for two historical earthquakes in AD 638 and 952. Quat. Inter., 371, 290-299, https://doi.org/10.1016/j.quaint.2014.09.045, 2015.

Zhang, F., Jin, Z.D., West, A.J., An, Z.S., Hilton, R.G., Wang, J., Li, G., Densmore, A.L., Yu, J.M., Qiang, X.K., Sun, Y.B., Li, L.B., Gou, L.F., Xu, Y., Xu, X.W., Liu, X.X., Pan, Y.H., You, C.F.: Monsoonal control on a delayed response of sedimentation to the 2008 Wenchuan earthquake. Sci. Adv., 5(6), eaav7110, https://doi.org/10.1126/sciadv.aav7110, 2019.

Zhang, P.Z., Deng, Q.D., Zhang, M.G., Ma, J., Gan, W.J., Wei, M., Mao, F.Y., Wang, Q.: Active tectonic blocks and strong earthquakes in the continent of China. Sci. China, 46, 13-24, https://doi.org/10.3969/j.issn.1674-7313.2003.z2.002, 2003.

Zhang, P.Z., Zhou, Z.Y., Xu, C.H., Zhang, Q.L.: Geochemistry of Pengguan complex in the Longmenshan region, western Sichuan Province, SW China: petrogenesis and tectonic implications. Geotecton. Metallog., 32(1), 105-116, https://doi.org/10.3969/j.issn.1001-1552.2008.01.014, 2008 (in Chinese).

Zhang, S.Q., Jiang, H.C., Fan, J.W., Xu, H.Y., Shi, W., Guo, Q.Q. and Wei, X.T.: Accumulation of a last deglacial gravel layer at Diexi, eastern Tibetan Plateau and its possible seismic significance. Front. Earth Sci., 9:797732, https://doi.org/10.3389/feart.2021.797732, 2021.

Zhang, Y.Q., Yang, N., Meng, H.: Deep-incised valleys along the Minjiang river upstream and their responses to the uplift of the West Sichuan Plateau, China. J. Chengdu Univ. Technol., 32(4), 331-339, https://doi.org/10.3969/j.issn.1671-9727.2005.04.001, 2005 (in Chinese).

Zhou R.J., Li, Y., Densmore, A.L., Ellis, M.A., He, Y.L., Wang, F.L., Li, X.G.: Active tectonics of the eastern margin of the Tibet Plateau. J. Mineral. Petrol., 26(2),40-51, https://doi.org/10.3969/j.issn.1001-6872.2006.02.007, 2006 (in Chinese).

Zhou, R.J., Pu, X.H., He, Y.L., Li, X.G., Ge, T.Y.: Recent activity of Minjiang fault zone, uplift of Minshan Block and their relationship with seismicity of Sichuan. Seism. Geol., 22(3),285-294, https://doi.org/CNKI:SUN:DZDZ.0.2000-03-009, 2000 (in Chinese).

Zhou, R.Y., Wen, X.Y., Lu, L., Li, Y.X., Huang, C.M.: Holocene paleosols and paleoclimate for the

906 arid upper Minjiang River valley in the eastern Tibetan Plateau. Catena, 206, 105555,

907 https://doi.org/10.1016/j.catena.2021.105555, 2021.

908 Zhong, N., Jiang, H.C., Li, H.B., Xu, H.Y., Shi, W., Zhang, S.Q., Wei, X.T.: Last Deglacial Soft-

909 Sediment Deformation at Shawan on the Eastern Tibetan Plateau and Implications for

910 Deformation Processes and Seismic Magnitudes. Acta Geol. Sinica, 93(2), 430-450,

911 https://doi.org/10.1111/1755-6724.13773, 2019.

912 Zhong, N., Song, X.S., Xu, H.Y., Jiang, H.C.: Influence of a tectonically active mountain belt on its

913 foreland basin: Evidence from detrital zircon dating of bedrocks and sediments from the eastern

914 Tibetan Plateau and Sichuan Basin, SW China. J. Asian Earth Sci., 146, 251-264,

915 https://doi.org/10.1016/j.jseaes.2017.05.035, 2017.

916 Zondervan, J., Stokes, M., Boulton, S., Telfer, M., Mather, A.: Rock strength and structural controls

917 on fluvial erodibility: Implications for drainage divide mobility in a collisional mountain belt.

918 Earth Planet. Sci. Lett., 538, 116221, https://doi.org/10.1016/j.epsl.2020.116221, 2020.